

## Research Articles





How to cite: *Angew. Chem. Int. Ed.* **2023,** *62*, e202218595 International Edition: doi.org/10.1002/anie.202218595 German Edition: doi.org/10.1002/ange.202218595

# Promoting Surface Electric Conductivity for High-Rate LiCoO<sub>2</sub>

Shenyang Xu, Xinghua Tan, Wangyang Ding, Wenju Ren, Qi Zhao, Weiyuan Huang, Jiajie Liu, Rui Qi, Yongxin Zhang, Jiachao Yang, Changjian Zuo, Haocheng Ji, Hengyu Ren, Bo Cao, Haoyu Xue, Zhihai Gao, Haocong Yi, Wenguang Zhao, Yinguo Xiao, Qinghe Zhao, Mingjian Zhang,\* and Feng Pan\*

Abstract: The cathode materials work as the host framework for both Li<sup>+</sup> diffusion and electron transport in Liion batteries. The Li<sup>+</sup> diffusion property is always the research focus, while the electron transport property is less studied. Herein, we propose a unique strategy to elevate the rate performance through promoting the surface electric conductivity. Specifically, a disordered rock-salt phase was coherently constructed at the surface of LiCoO<sub>2</sub>, promoting the surface electric conductivity by over one magnitude. It increased the effective voltage  $(V_{\rm eff})$  imposed in the bulk, thus driving more Li<sup>+</sup> extraction/insertion and making LiCoO<sub>2</sub> exhibit superior rate capability (154 mAh g<sup>-1</sup> at 10 C), and excellent cycling performance (93 % after 1000 cycles at 10 C). The universality of this strategy was confirmed by another surface design and a simulation. Our findings provide a new angle for developing high-rate cathode materials by tuning the surface electron transport property.

#### Introduction

For the rapidly iterating portable electronics, high-energy-density and high-rate cathode materials are required for Liion batteries. Lithium cobalt oxide (LCO) is the most successful cathode material for Li-ion batteries in portable electronics. The charging cutoff voltage of commercial LCO is usually restricted to 4.2 V, delivering a low capacity

of  $\approx 140 \text{ mAh g}^{-1}$  (Li<sub>1-x</sub>CoO<sub>2</sub>,  $x \approx 0.5$ ,  $\approx 4.2 \text{ V}$  vs. Li/Li<sup>+</sup>), half of the theoretical capacity of 274 mAh g<sup>-1</sup>. [1e,2] To meet the demand for higher energy density, increasing the charging cut-off voltage to extract more Li+ is one of the most common ways. Nevertheless, it brings another concern, the poor cycling stability. One reason is that the highlyactive  $Co^{4+}$  and  $O^{n-}$  (n < 2) species formed under high operating voltage would react with the electrolyte, resulting in Co dissolution and surface structure degradation.[3] Another reason is the severe lattice mismatch due to the O3-H1-3 phase transition above 4.5 V, resulting in huge internal strain and the structure collapse.<sup>[4]</sup> Various coating and doping methods have been developed to solve the concern, including aluminum-containing materials (e.g., Al<sub>2</sub>O<sub>3</sub>, AlF<sub>3</sub>) coating,<sup>[5]</sup> Li&Al-containing materials coating such as LAGP, [4a] LATP, [6] and LiAlF4 and elemental doping with Ti, [7] Mg, [7a,8] Al, [2] Ni, [9] etc. These strategies enhanced the cycling stability of LCO by varied extents, but ignored the influences on other performances, especially the rate capability.

In work mentioned above, one strange phenomenon is noticed: although the cutoff voltage is set the same for LCO, there are significant differences in the specific capacity under the same voltage range. As shown in Figure 1a–b, the discharge capacities at 0.1 C under the upper cutoff voltages of 4.5 and 4.6 V are summarized, showing great differences of about 30 mAh g<sup>-1</sup>, respectively. Such big differences in capacity may be related with the different treatments, which, although they partially improved the cycling stability, sacrificed the capacity and energy density, thus defending the original intention: improving the energy density through

[\*] S. Xu, X. Tan, W. Ding, Q. Zhao, W. Huang, J. Liu, H. Ji, H. Ren, B. Cao, H. Xue, Z. Gao, H. Yi, W. Zhao, Y. Xiao, Q. Zhao, M. Zhang,

School of Advanced Materials, Peking University

Shenzhen Graduate School

Shenzhen 518055 (P. R. China)

E-mail: panfeng@pkusz.edu.cn

W. Ren

School of Advanced Manufacturing Engineering, Chongqing University of Posts and Telecommunications

Chongqing 400065 (China)

R. Qi

Department of Materials, University of Oxford 16 Parks Road, Hume-Rothery Building, Oxford (UK) Y. Zhang

School of Chemistry and Chemical Engineering, Guangxi University Nanning 530004 (China)

J. Yang

School of Metallurgy and Environment, Central South University Changsha 410083 (China)

C 7uo

Department of Mechanical and Automation Engineering, The Chinese University of Hong Kong Hong Kong SAR (China)

M 7hang

School of Science and Engineering, The Chinese University of Hong Kong

Shenzhen 518172 (China)

E-mail: zhangmingjian@cuhk.edu.cn

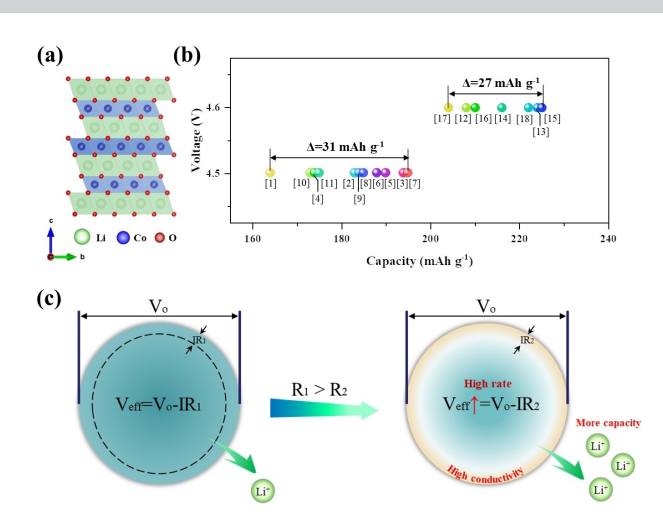


Figure 1. (a) The layered structure of LCO. (b) The initial discharge capacities of reported LCO at 0.1 C at the upper cutoff voltages 4.5 and 4.6 V (the references are deposited in Table S1). (c) Schematic illustration of the strategy to improve the rate performance of cathode materials through tuning surface electric conductivity.

elevating the cutoff potential. One typical example is that the cutoff voltage was improved to 4.7 V, while the capacity is still 230 mAh g<sup>-1</sup>, [10] equivalent to those using the cutoff voltage of 4.6 V. Why was the rate performance partially damaged in these reports? After carefully examining the experimental details, we found two possible reasons. The first one is the difference in the technological processes including the material preparation, the slurry preparation, electrode preparation and the cycling conditions. The second one is that the surface modification strategy or elemental doping alters the surface structure, thus affecting the surface electron/Li+ conductivity.[11] The latter is more probable since various modifications are applied. From the aspect of surface electron transport, one possible mechanism is proposed here (Figure 1c). Generally, the extraction/ insertion of Li ions inside the single particle are driven by the impressed effective potential  $(V_{\rm eff})$ , where  $V_{\rm eff}$  is determined by the potential applied on each particle  $(V_o)$ and the potential drop (IR) due to the surface resistance (R). If the R value is increased,  $V_{\rm eff}$  is lower, and the available Li ions would be reduced. In other words, the rate performance should be greatly affected by the surface electric conductivity. Following this logic, the reported modifications above may damage the surface electric conductivity, thus lowering the rate performance, which explains the phenomenon above. Accordingly, we could improve the rate performance of cathodes by increasing the surface electric conductivity.

Herein, we constructed a (Li/Co/Al)(O/F) surface layer with the unique disordered rock-salt structure at the surface of LCO through low-speed ball milling, which can significantly enhanced the surface electric conductivity compared with bare LCO, thus elevating the effective potential  $V_{\rm eff}$ , eventually delivering the best rate performance ever at 4.5 V. In addition, the intrinsic structure stability of rock-salt phase effectively suppressed the surface electrochemical

reactions to protect the inner layered framework within the particle, thus showing superior cycling stability at high rate up to 10 C. These findings highlight the importance of tuning surface electron transport property in pursuing high-rate cathode materials.

#### **Results and Discussion**

LCO with the typical layered structure (Figure 2a) was chosen to do the surface modification for improving the surficial electric conductivity (Figure S1a, see details in Experimental section). The modified LCO samples were marked as LCO-M1, LCO-M2, LCO-M3, respectively, according to the different usages of additives. As shown in Figure S1b, there is no new peak observed in X-ray diffraction (XRD) patterns, indicating that the bulk structure is intact after treatment, and still preserves the typical layered structure (space group  $R\bar{3}m$ , JCPDS no. 44-0145). [12] Rietveld refinements of XRD patterns demonstrate the lattice parameters slightly increase after modification (Figure S2 and Table S2). The similar X-ray pair distribution

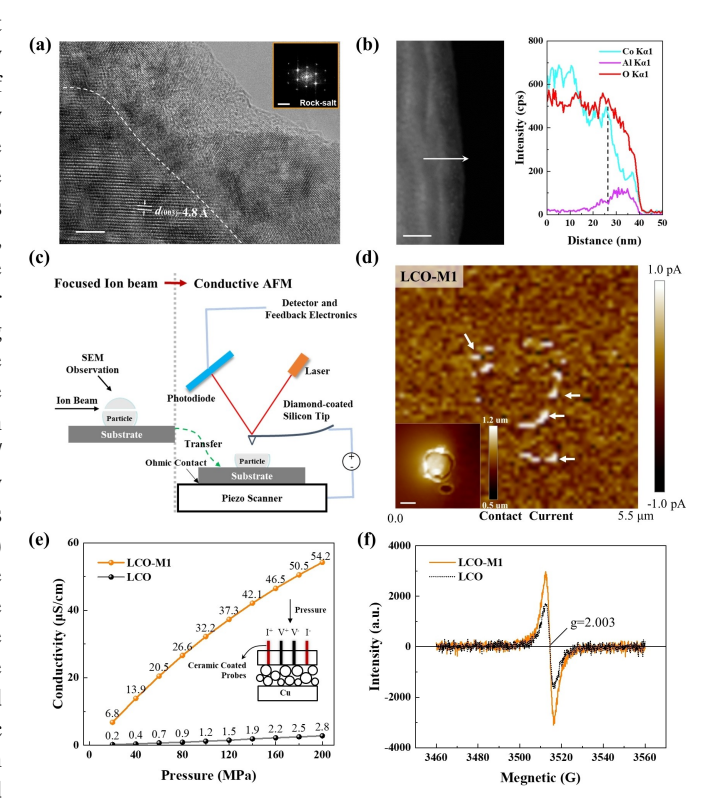


Figure 2. Improved surface conductivity. (a) HRTEM image of LCO-M1 and the selected-area FFT map. The scale bars of HRTEM image and FFT map are 5 nm and 5 1/nm, respectively. (b) TEM image of LCO-M1 and the corresponding EDX line scanning results along the arrow in TEM image. (c) Schematic diagram of AFM conductivity test on the cross-section sample of the individual particle. (d) The AFM contact current images of cross section sample of the individual particle. The inset is the corresponding height image. The scale bar is 1  $\mu$ m. (e) The electric conductivity of LCO and LCO-M1 powders under different pressures measured by four-probes method. (f) The EPR spectra of LCO and LCO-M1.





function (PDF) patterns of LCO and LCO-M1 indicate that surface modification does not affect the local structure of the particles (Figure S3). The scanning electron microscope (SEM) images (Figure S4) indicate that, the surface becomes rougher with the additives' content increase. The corresponding EDS results (Figure S4 and Table S3) prove the relative uniformity of the surface modification.

Transmission electron microscopy (TEM) and X-ray photoelectron spectroscopy (XPS) were further performed to examine the surface structure. In Figure 2a, the bulk of LCO-M1 particle still maintains the layered structure, while the surface is covered by the island-like nanoparticles featuring a rock-salt phase (see the corresponding FFT map) and the amorphous species in the thickness of 5-20 nm. TEM EDX line scan was performed to check the elemental compositions of these surface species. As shown in Figure 2b, Al concentrated on the surface region (divided by the vertical dashed line) and gradually decreased into the bulk spanning around 20 nm. In the same surficial region, the Co concentration is about 1/3 of that in the bulk, which corresponds to the surficial rock salt structure. XPS was carried out to detect F element. In F 1s XPS spectra, the intensity of F signal gradually decreases with the depth, indicating a concentration gradient of F content from the surface to the bulk (Figure S5). In Co 2p XPS spectra, a bigger satellite peak at 785 eV is attributed to Co<sup>2+</sup> for LCO-M1 (Figure S6). It indicates the increase of Co<sup>2+</sup> content in LCO-M1, which should be related with Fsubstitution with O<sup>2-</sup> at the surface.<sup>[13]</sup> Combining this information together, the surface layer can be deduced as rock-salt-like (Li, Co, Al)(O,F) analogue to NiO-type

To evaluate the effect of the surface modification on the electric conductivity, we studied the electric conductivity of LCO and LCO-M1 on the individual particle and the powder using the atomic force microscope (AFM) and the four-probes method, respectively. The height and the contact current images by AFM are shown in Figure S7. LCO-M1 particle shows the higher brightness than the LCO particle, hinting at the higher surface conductivity of the whole modified LCO particle. We further combined focused ion beam (FIB) and AFM to measure the electric conductivity on the cross-section of the individual particle (Figure 2c). As shown in Figure 2d, the contrast at the particle surface is much brighter than that in bulk compared with LCO (Figure S8), which fully proves that a highly conductive surface is obtained on LCO-M1.

The electric conductivity measurements of the powder were performed under different pressures (see details in Table S4). As shown in Figure 2e, the conductivities of bare LCO and LCO-M1 show the same linear increasing trend with the pressure, which should be related with the increasing compact density. In the whole pressure range of 20–200 MPa, LCO-M1 has a conductivity one order of magnitude higher than bare LCO, and the highest conductivity of LCO-M1 can reach 54.2 µS cm<sup>-1</sup> under 200 MPa. In addition, we measured the resistances of four cathode electrodes directly. As shown in Figure S9, the modified LCO electrodes show smaller resistivities of 0.0092, 0.0086,

and  $0.0072~\Omega$ cm compared with the bare LCO electrode  $(0.0126~\Omega$ cm), reflecting a better conductive network benefitting from the surface modification of cathode materials. All these data confirm the significant improvement of the electric conductivity in LCO by surface modification. The electron paramagnetic resonance (EPR) test was performed to explore the reason for the improved conductivity. As shown in Figure 2f, LCO-M1 exhibits a stronger signal at g=2.003 than LCO, hinting at the formation of more oxygen vacancy defects in LCO-M1. It may be due to the cationic/anionic disordering in the surface region, and can be responsible for the improved electric conductivity. Overall, the surface-treated LCO becomes highly conductive due to the surface's disordered rock salt (Li, Co,Al)(O,F) structure.

To validate the relationship between surface conductivity and the rate performance proposed above, we systemically compare the electrochemical performance of LCO and LCO-M1 with better surface conductivity (Figure 3a–d, S10–S15). Figure 3a presents the capacity-voltage profiles in 3.0–4.5 V at 0.1 C (1 C=200 mA g<sup>-1</sup>). The charge curve of LCO-M1 is underneath that of LCO, while the discharge curve of LCO-M1 is above that of LCO, indicating more negligible polarization and higher capacity (195 vs. 180 mAh g<sup>-1</sup>) of

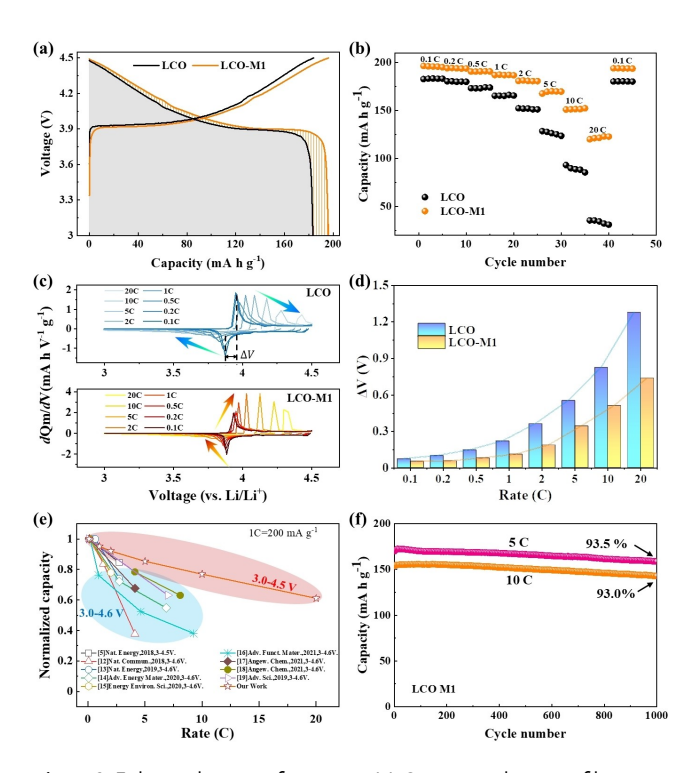


**Figure 3.** Enhanced rate performance. (a) Capacity-voltage profiles during the second cycle of LCO and LCO-M1 in 3.0–4.5 V at 0.1 C. (b) The rate performance of LCO and LCO-M1 in 3.0–4.5 V at 25 °C. (c) The dQm/dV curves of LCO and LCO-M1 at different rates in 3.0–4.5 V. The arrows show the change trends of the redox peaks. (d) The plot of  $\Delta V$  as a function of the rate.  $\Delta V$  is defined as the voltage difference of the charge peak and discharge peak in the dQm/dV curves for quantifying the polarization change. (e) The comparison of the rate performance between LCO-M1 and the reported LCO cathodes. The references are listed in Table S1. (f) Cycling performance of LCO-M1 in the voltage range of 3–4.5 V at 5 C and 10 C.

LCO-M1 due to the improved surface conductivity and effective voltage ( $V_{\rm eff}$ ). A similar phenomenon was observed when the cut-off voltage was raised to 4.55 V (Figure S10a). The discharge energy density of LCO-M1 reached 853 W h kg<sup>-1</sup> in 3–4.55 V in the second cycle, superior to that of bare LCO (782 W h kg<sup>-1</sup>).

As expected, improved electric conductivity extensively promotes the rate performance. As shown in Figure 3b, LCO-M1 has much higher capacities than LCO at various rates in 3-4.5 V. Especially it delivers a capacity of 120 mAh g<sup>-1</sup> at 20 C, much larger than those of LCO, LCO-M2, and LCO-M3 (36, 89, and 73 mAh g<sup>-1</sup>, respectively) (Figure S11). A similar phenomenon was observed in 3.0-4.45 V (Figure S12a). When the cut-off voltage is increased to 4.55 or 4.6 V, the increase in capacity is not so apparent, which may be related with the irreversible O redox above 4.5 V (Figure S12b and S13). Figure 3c present the corresponding dQm/dV curves at different rates. A parameter  $\Delta V$ , defined as the voltage difference between the charge peak and the discharge peak, was introduced to quantify the degree of charge-discharge polarization with the rate. As shown in Figure 3d, the  $\Delta V$  value of LCO-M1 is only 0.74 V at 20 C, nearly half that of LCO (1.28 V). It further confirms that improving the surface conductivity significantly reduces the polarization at different rates. We compared the rate performance of the reported LCO cathodes modified by various methods in Figure 3e. The modified LCO in our work exhibits the better rate than others.

In addition, the long cycling stability was also greatly promoted (Figure 3f and Figure S14-S15). In 3.0-4.5 V, LCO-M1 displays the capacity retentions of 96.8 % after 100 cycles at 0.2 C, 93.8 % after 500 cycles at 1 C, 93.5 % and 93.0% after 1000 cycles at 5 C and 10 C, respectively. In 3.0-4.55 V, LCO-M1 can maintain a specific capacity of 141 mAh g<sup>-1</sup> after 1500 cycles at 3 C, equivalent to a capacity retention rate of 81.6%, sharply in contrast to LCO (8.5%, Figure S15). The excellent cycling stability should benefit from the intrinsic structure stability of the surface rock salt phase, which is demonstrated by maintaining the rock-salt surface structure in the TEM images of LCO-M1 charged to 4.5 V and after 300 cycles (Figure S16-S17). In addtion, time-of-flight secondary-ion mass spectrometry (ToF-SIMS) demonstratres (Figure S18), LCO-M1 has a more uniform cathode electrolyte interphase (CEI) layer mainly composited with LiF2- and other inorganic species. [14] It should be related to the higher surface electric conductivity, [15] and could effectively suppresses side reactions and lattice oxygen loss, confirmed by differential electrochemical mass spectrometry (DEMS) (Figure S19).

In brief, benefitting from the high surface conductivity and the intrinsic stable structure of the disordered rock-salt phase, the modified LCO shows both ultrahigh rate performance and long cycle stability.

Li<sup>+</sup> diffusion was another critical factor to affect the rate performance of LCO. Here the Li<sup>+</sup> diffusion kinetics was quantified by electrochemical impedance spectroscopy (EIS) and galvanostatic intermittent titration techniques (GITT). The EIS spectra of LCO and LCO-M1 are presented in Figure 4a. LCO-M1 exhibits a lower interface

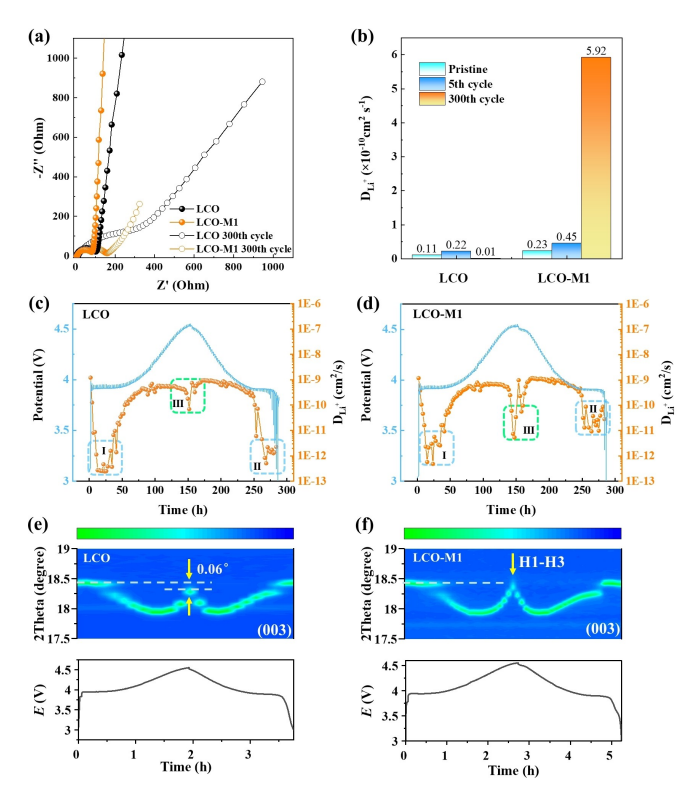


**Figure 4.** The impact of electron conductivity on Li<sup>+</sup> diffusion and phase transition. (a) Electrochemical impedance spectra of LCO and LCO-M1 before cycling and after 300 cycles in 3–4.5 V at 1 C. (b) The Li<sup>+</sup> diffusion coefficients ( $D_{\text{Li}+}$ ) of LCO and LCO-M1 derived from the fitting of EIS spectra in (a). GITT measurements of LCO (c) and LCO-M1 (d) during the initial charge/discharge. In situ XRD evolution of bare LCO (e) and LCO-M1 (f) at the (003) peak with the corresponding electrochemical curves.

impedance than LCO before cycling and after 300 cycles. Through the equivalent circuit fitting, the surface film resistance  $(R_f)$ , the charge transfer impedance  $(R_{ct})$ , and the Li<sup>+</sup> diffusion coefficients can be deduced (Figure S21–S22 and Table S5). The impedance  $(R_f+R_{ct})$  of LCO-M1 increased from 82 to  $145\,\Omega$  after 300 cycles, while the impedance of LCO increased from 90 to 263  $\Omega$ . The results may relate with the reduced surface structural degradation by the stable disordered rock-salt surface. As shown in Figure 4b, the  $Li^+$  diffusion coefficients ( $D_{Li+}$ ) of LCO-M1 is  $0.23 \times 10^{-10} \text{ cm}^2 \text{ s}^{-1}$ , twice that of LCO  $(0.11 \times 10^{-10} \text{ cm}^2 \text{ s}^{-1})$ . Shockingly, it increased by 25 times  $(5.92 \times 10^{-10} \text{ cm}^2 \text{ s}^{-1})$ after 300 cycles, while that of LCO decreased to 0.01× 10<sup>-10</sup> cm<sup>2</sup> s<sup>-1</sup>. These results indicate that the ordered Li<sup>+</sup> transport channels favoring rapid Li<sup>+</sup> (de)intercalation formed in LCO-M1 after cycling. Furthermore, combined characterizations of SEM coupled with FIB and EDX ((Figure S23), ToF-SIMS (Figure S24) and distribution of relaxation time (DRT) analysis of impedance spectra (Figure S25)  $^{\left[14,17\right]}$  demonstrate that the increased Li  $^{+}$  diffusion may come from the dense and stable CEI layer that allows both Li<sup>+</sup> and electrons to pass through quickly.

GITT measurements were further conducted to evaluate the  ${\rm Li}^+$  diffusion during charge/discharge. Figure 4c-d

present the charge/discharge curves of LCO and LCO-M1 along with the corresponding  $D_{\mathrm{Li}_{+}}$  values. Overall, LCO-M1 has higher D values than LCO-M1 except in region III. They both exhibit region I and region II with low  $D_{\text{Li}+}$ values during the initial charge section and the final discharge section (marked by the blue shadows), which is consistent with the previous reports, and related to the formation of H2 phase with the poor Li+ transport capability due to the narrowed interlayer spacing. [1e,18] Differently, the  $D_{\mathrm{Li}+}$  values of LCO-M1 in region II are nearly one order of magnitude higher than those of LCO, which benefits the rate performance. Another noticeable difference is found in region III (marked by the green shadows). The low  $D_{\text{Li}+}$  values appeared in region III of LCO-M1, accompanying with a voltage plateau above 4.5 V coming from the O redox behavior. It corresponds to the deeper phase transition to H1-3 phase (demonstrated by in situ XRD as below) involving O redox in LCO-M1, thus leading to the slower Li<sup>+</sup> diffusion kinetics.<sup>[19]</sup> A similar phenomenon can be observed in the second cycle (Figure S26).

Since the electrochemical reaction process of LiCoO<sub>2</sub> is strongly associated with structural evolution, in situ XRD experiments were performed to study the phase evolution of LCO and LCO-M1 during charge/discharge. As shown in Figure 4e-f, the (003) peak presents similar shift trends for LCO and LCO-M1. It initially shifts to a high angle, then to the low angle, indicating a series of phase transitions from H1 to H2, to M1, to H3. When charged to 4.55 V, LCO still preserved the H3 phase, while LCO-M1 underwent a phase transition from H3 to H1-H3, which is consistent with the higher capacity of LCO-M1 (Figure S10a) and the reversible O redox peaks at around 4.5 V (Figure S10b), and reasonably explains the low D values in the region III of LCO-M1 (Figure 4d). The phenomenon originates from the better surficial conductivity of LCO-M1 and the higher effective voltage, which make the phase transition happen at the lower applied voltage.

Furthermore, Co *L*-edge and O *K*-edge soft X-ray absorption spectra (sXAS) were collected to track the changes in chemical state. As shown in Figure S27, peak A (  $\approx$ 778 eV) and B ( $\approx$ 780 eV) are assigned to Co<sup>2+</sup> and Co<sup>3+</sup>, respectively. Co<sup>2+</sup> comes from the Co<sub>3</sub>O<sub>4</sub>-like spinel-phase formed during the charge, [20] which is confirmed by the Raman spectra (Figure S28). [21] The formation of Co<sup>2+</sup> and spinel phase in LCO-M1 is earlier than in LCO, consistent with the early phase transtion. As shown in Figure S29, the peak around 531.5 eV marked by the arrows can be assigned to the oxidized O species. LCO-M1 has a higher peak than LCO at 4.5 V, suggesting more oxygen oxidation involved in LCO-M1, consistent with the higher capacity.

Finally, we use a scheme (Figure 5) to depict the mechanism of the improved electrochemistry. There are three characteristics for the disordered rock-salt surface: ① Stable framework. Rock-salt phase has the most stable anionic framework compared to the layered or spinel phase. ② Good Li<sup>+</sup> percolation. Extensive works by Ceder et al. show that the rational construction of the rock salt enables the material to have a good Li<sup>+</sup> percolation network and

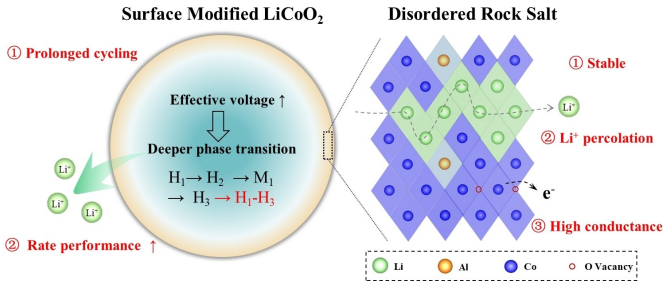


**Figure 5.** Schematic diagram of high-rate material design. Surface structure with high stability and Li<sup>+</sup> diffusion kinetics for stable long-cycle and variable high-rate electrochemical performance.

support the macroscopic migration of Li<sup>+</sup>.<sup>[22]</sup> The disordered rock salt materials always have a lower voltage during delithiation in their disordered form, while they have a higher voltage during lithiation in their disordered form.<sup>[23]</sup>

③ High electric conductivity. The stable structure protects the inside layered lattice, and ensures prolonged cycling. The disordering occupancy of heterovalent cations (Li<sup>+</sup>/Co<sup>2+</sup>/Co<sup>3+</sup>/Al<sup>3+</sup>) and anions (O<sup>2-</sup>/F<sup>-</sup>) in the rock-salt structure, may create the abundant O vacancies and the smooth electron transport at the surface, which increase the effective voltage imposed on the layered lattice inside, and lead to the deeper phase transition, thus extracting/inserting more Li ions under the same external voltage range, namely elevating the rate performance.

All these results above confirm our initial strategy (Figure 1c): promote the rate performance of cathodes by increasing the surficial electric conductivity. For further verify the universality of electric and ionic conductivity was adopted for the surface modification of LCO.<sup>[24]</sup> It also exhibits ultra-high rate performance (Figure S30), even better than LCO-M1. The discharge specific capacity reaches 150 mAh g<sup>-1</sup> at 20 C in 3.0–4.5 V.

To further elucidate the effect of the surface electric conductivity on the ionic conductivity, we simulate the electrochemical process with a finite-element model (Figure 6a). The model consists of three parts, a spherical particle of LiCoO<sub>2</sub> with a diameter of 10 microns, a thin conductive layer covering half a sphere, and an electrolyte with boundary condition. The conductivity of the conductive layer is set as 0.2 and 6.8 μS cm<sup>-1</sup>, respectively, according to the experimental results of LCO and LCO-M1 (see details in Supporting Information). It is clear, LCO with the higher surface conductivity presents a longer discharge time than LCO (Figure 6b), corresponding to the larger specific capacity, as evidenced by the experimental result. As shown in Figure 6c, the particle with a higher surface conductivity also shows a more uniform surface potential distribution and higher potential in the end of discharge (30s and 35s), making the Li+ inside the particle diffuse faster. Moreover, the Li<sup>+</sup> concentration distributions at different discharging times (Figure 6d-g and S31-S32) further confirm that the high surface conductivity facilitates the fast Li<sup>+</sup> insertion.

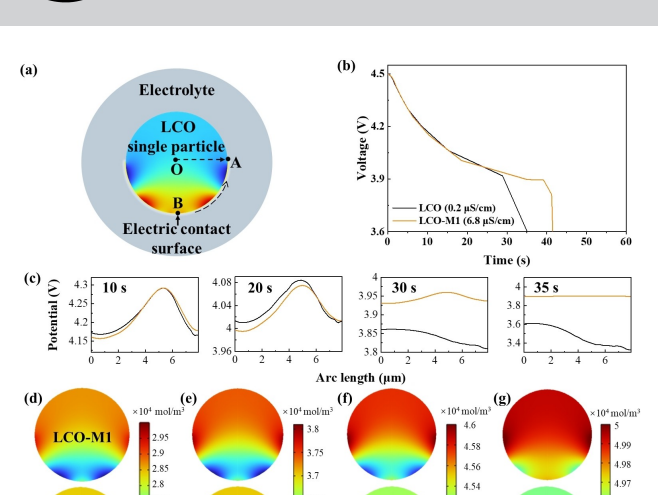


**Figure 6.** The impact of surface electric conductivity on the electrochemical performance by a finite-element simulation. (a) The model for the finite element simulation. (b) The discharge curves of LCO with low and high surface conductivities. (c) Surface potential distribution along the  $\widehat{BA}$  arc (marked in (a)) when discharging at 10, 20, 30 and 35 s. Li<sup>+</sup> concentration distribution at 5 (d), 10 (e), 20 (f), and 30 (g) s.

4.52 4.5

### Conclusion

In summary, we proposed a unique strategy to increase the rate performance of cathodes by promoting the surface electric conductivity. To validate the strategy, we constructed a disordered rock-salt type (Li/Al/Co)(O/F) layer at the surface of LCO cathode. The conductivity tests on a single particle, powder and electrode samples demonstrated that, the electron conductivity was improved by over one order of magnification. It significantly increased the effective voltage imposed in the bulk of individual particles and drove more Li<sup>+</sup> extraction/insertion under the same external Eventually, a superior voltage. rate performance (154 mAh g<sup>-1</sup> at 10 C in 3.0-4.5 V) was achieved, accompanied with the excellent cycling performance (capacity retention of 93.0% at 10 C after 1000 cycles) benefitting from the intrinsic structural stability of the rock-salt surface and the uniform and dense CEI layer. The property of Li<sup>+</sup> extraction/insertion in the cathodes is correlated with the surface electron transport property through the new concept of the effective voltage  $V_{\rm eff}$  for the first time here. These findings deepen the understanding of electron/Li<sup>+</sup> transport properties in cathode materials and open a new direction to develop fast charging/discharging cathodes. The surface and bulk conductivity evolution during the charge/discharge process and the influences on the electrochemical performance deserve further studies.

#### Acknowledgements

This work was financially supported by the National Natural Science Foundation of China (52172175), the Shenzhen

Technology Science and Research Grant (JCYJ20210324130812033, JCYJ20200109140416788, GXWD20201231165807007-20200807111854001), Soft Science Research Project of Guangdong Province (No. 2017B030301013), the Basic and Applied Basic Research Foundation of Guangdong Province 2021B1515130002), the National Key R&D Program of China (2020YFB0704500), and the Major Science and Technology Infrastructure Project of Material Genome Bigscience Facilities Platform supported by Municipal Development and Reform Commission of Shenzhen.

## **Conflict of Interest**

The authors declare no conflict of interests.

### **Data Availability Statement**

The data that support the findings of this study are available from the corresponding author upon reasonable request.

**Keywords:** Effective Voltage · Electric Conductivity · High Rate · LiCoO<sub>2</sub> · Surface Structure

- a) Y. Y. Jiang, P. F. Yan, M. C. Yu, J. M. Li, H. Jiao, B. Zhou, M. L. Sui, Nano Energy 2020, 78, 105364; b) S. C. Song, Y. W. Li, K. Yang, Z. F. Chen, J. J. Liu, R. Qi, Z. B. Li, C. J. Zuo, W. G. Zhao, N. Yang, M. J. Zhang, F. Pan, J. Mater. Chem. A 2021, 9, 5702–5710; c) T. Liu, F. Pan, K. Amine, Chin. J. Struct. Chem. 2020, 39, 11–15; d) E. Zhitao, H. Guo, G. Yan, J. Wang, R. Feng, Z. Wang, X. Li, J. Energy Chem. 2021, 55, 524–532; e) Y. Lyu, X. Wu, K. Wang, Z. Feng, T. Cheng, Y. Liu, M. Wang, R. Chen, L. Xu, J. Zhou, Y. Lu, B. Guo, Adv. Energy Mater. 2021, 11, 2000982.
- [2] Q. Liu, X. Su, D. Lei, Y. Qin, J. Wen, F. Guo, Y. A. Wu, Y. Rong, R. Kou, X. Xiao, F. Aguesse, J. Bareño, Y. Ren, W. Lu, Y. Li, *Nat. Energy* 2018, 3, 936–943.
- [3] J. Qian, L. Liu, J. Yang, S. Li, X. Wang, H. L. Zhuang, Y. Lu, Nat. Commun. 2018, 9, 4918.
- [4] a) Z. Li, A. Li, H. Zhang, F. Ning, W. Li, A. Zangiabadi, Q. Cheng, J. J. Borovilas, Y. Chen, H. Zhang, X. Xiao, C. Ouyang, X. Huang, W.-K. Lee, M. Ge, Y. S. Chu, X. Chuan, Y. Yang, Energy Storage Mater. 2020, 29, 71–77; b) J. Li, C. Lin, M. Weng, Y. Qiu, P. Chen, K. Yang, W. Huang, Y. Hong, J. Li, M. Zhang, C. Dong, W. Zhao, Z. Xu, X. Wang, K. Xu, J. Sun, F. Pan, Nat. Nanotechnol. 2021, 16, 599–605; c) A. Van der Ven, M. K. Aydinol, G. Ceder, G. Kresse, J. Hafner, Phys. Rev. B 1998, 58, 2975–2987.
- [5] a) A. Yano, M. Shikano, A. Ueda, H. Sakaebe, Z. Ogumi, J. Electrochem. Soc. 2017, 164, A6116–A6122; b) J. Xie, A. D. Sendek, E. D. Cubuk, X. Zhang, Z. Lu, Y. Gong, T. Wu, F. Shi, W. Liu, E. J. Reed, Y. Cui, ACS Nano 2017, 11, 7019–7027; c) L. Wang, B. Chen, J. Ma, G. Cui, L. Chen, Chem. Soc. Rev. 2018, 47, 6505–6602.
- [6] Y. Wang, Q. Zhang, Z. Xue, L. Yang, J. Wang, F. Meng, Q. Li, H. Pan, J. Zhang, Z. Jiang, W. Yang, X. Yu, L. Gu, H. Li, Adv. Energy Mater. 2020, 10, 2001413.
- [7] a) J.-N. Zhang, Q. Li, C. Ouyang, X. Yu, M. Ge, X. Huang, E.
   Hu, C. Ma, S. Li, R. Xiao, W. Yang, Y. Chu, Y. Liu, H. Yu, X. Q. Yang, X. Huang, L. Chen, H. Li, *Nat. Energy* 2019, 4, 594–

- 603; b) T. Tian, T. W. Zhang, Y. C. Yin, Y. H. Tan, Y. H. Song, L. L. Lu, H. B. Yao, *Nano Lett.* **2020**, 20, 677–685; c) Y. Hong, X. Huang, C. Wei, J. Wang, J.-N. Zhang, H. Yan, Y. S. Chu, P. Pianetta, R. Xiao, X. Yu, Y. Liu, H. Li, *Chem* **2020**, 6, 2759–2769.
- [8] Y. Y. Huang, Y. C. Zhu, H. Y. Fu, M. Y. Ou, C. C. Hu, S. J. Yu, Z. W. Hu, C. T. Chen, G. Jiang, H. K. Gu, H. Lin, W. Luo, Y. H. Huang, Angew. Chem. Int. Ed. 2021, 60, 4682–4688; Angew. Chem. 2021, 133, 4732–4738.
- [9] M. Hirooka, T. Sekiya, Y. Omomo, M. Yamada, H. Katayama, T. Okumura, Y. Yamada, K. Ariyoshi, J. Power Sources 2020, 463, 228127.
- [10] X. Yang, C. Wang, P. Yan, T. Jiao, J. Hao, Y. Jiang, F. Ren, W. Zhang, J. Zheng, Y. Cheng, X. Wang, W. Yang, J. Zhu, S. Pan, M. Lin, L. Zeng, Z. Gong, J. Li, Y. Yang, *Adv. Energy Mater.* 2022, 12, 2200197.
- [11] a) W. Ren, K. Wang, J. Yang, R. Tan, J. Hu, H. Guo, Y. Duan, J. Zheng, Y. Lin, F. Pan, J. Power Sources 2016, 331, 232–239;
  b) Z. Wu, X. Han, J. Zheng, Y. Wei, R. Qiao, F. Shen, J. Dai, L. Hu, K. Xu, Y. Lin, W. Yang, F. Pan, Nano Lett. 2014, 14, 4700–4706.
- [12] D. Wang, X. Ma, Y. Wang, L. Wang, Z. Wang, W. Zheng, X. He, J. Li, Q. Peng, Y. Li, *Nano Res.* 2010, 3, 1–7.
- [13] L. Dahéron, R. Dedryvère, H. Martinez, M. Ménétrier, C. Denage, C. Delmas, D. Gonbeau, *Chem. Mater.* 2008, 20, 583–590.
- [14] W. Liu, J. Li, W. Li, H. Xu, C. Zhang, X. Qiu, Nat. Commun. 2020, 11, 3629.
- [15] S. Zhang, R. Li, N. Hu, T. Deng, S. Weng, Z. Wu, D. Lu, H. Zhang, J. Zhang, X. Wang, L. Chen, L. Fan, X. Fan, *Nat. Commun.* 2022, 13, 5431.
- [16] a) Z. Feng, R. Rajagopalan, D. Sun, Y. Tang, H. Wang, Chem. Eng. J. 2020, 382, 122959; b) L. Li, Z. Chen, Q. Zhang, M. Xu, X. Zhou, H. Zhu, K. Zhang, J. Mater. Chem. A 2015, 3, 894– 904.
- [17] a) Y. Lu, C. Zhao, J. Huang, Q. Zhang, *Joule* **2022**, 6, 1172–1198; b) T. H. Wan, M. Saccoccio, C. Chen, F. Ciucci, *Electrochim. Acta* **2015**, *184*, 483–499; c) X. Wang, C. Chen, S. Wu, H.

- Zheng, Y. Chen, H. Liu, Y. Wu, H. Duan, *Energy Technol.* **2022**, *10*, 2100841.
- [18] J. Xie, N. Imanishi, T. Matsumura, A. Hirano, Y. Takeda, O. Yamamoto, Solid State Ionics 2008, 179, 362–370.
- [19] S. Kaewmala, W. Limphirat, V. Yordsri, H. Kim, S. Muhammad, W. S. Yoon, S. Srilomsak, P. Limthongkul, N. Meethong, Sci. Rep. 2019, 9, 427.
- [20] a) F. Morales, F. M. F. de Groot, P. Glatzel, E. Kleimenov, H. Bluhm, M. Haevecker, A. Knop-Gericke, B. M. Weckhuysen, J. Phys. Chem. B 2004, 108, 16201–16207; b) F. Lin, I. M. Markus, D. Nordlund, T.-C. Weng, M. D. Asta, H. L. Xin, M. M. Doeff, Nat. Commun. 2014, 5, 3529; c) M. Ghiasi, M. U. Delgado-Jaime, A. Malekzadeh, R.-P. Wang, P. S. Miedema, M. Beye, F. M. F. de Groot, J. Phys. Chem. C 2016, 120, 8167–8174.
- [21] a) X. Cao, H. Li, Y. Qiao, M. Jia, X. Li, J. Cabana, H. Zhou, Adv. Mater. 2020, 32, 2004280; b) A. Vandenberg, A. Hintennach, Russ. J. Electrochem. 2015, 51, 310–317.
- [22] a) J. Lee, A. Urban, X. Li, D. Su, G. Hautier, G. Ceder, Science 2014, 343, 519–521; b) H. Ji, J. Wu, Z. Cai, J. Liu, D.-H. Kwon, H. Kim, A. Urban, J. K. Papp, E. Foley, Y. Tian, M. Balasubramanian, H. Kim, R. J. Clément, B. D. McCloskey, W. Yang, G. Ceder, Nat. Energy 2020, 5, 213–221; c) Z. Cai, H. Ji, Y. Ha, J. Liu, D.-H. Kwon, Y. Zhang, A. Urban, E. E. Foley, R. Giovine, H. Kim, Z. Lun, T.-Y. Huang, G. Zeng, Y. Chen, J. Wang, B. D. McCloskey, M. Balasubramanian, R. J. Clément, W. Yang, G. Ceder, Matter 2021, 4, 3897–3916; d) R. J. Clément, Z. Lun, G. Ceder, Energy Environ. Sci. 2020, 13, 345–373; e) A. Urban, J. Lee, G. Ceder, Adv. Energy Mater. 2014, 4, 1400478.
- [23] A. Abdellahi, A. Urban, S. Dacek, G. Ceder, *Chem. Mater.* 2016, 28, 3659–3665.
- [24] M. Yoon, Y. Dong, J. Hwang, J. Sung, H. Cha, K. Ahn, Y. Huang, S. J. Kang, J. Li, J. Cho, Nat. Energy 2021, 6, 362–371.

Manuscript received: December 16, 2022 Accepted manuscript online: January 2, 2023 Version of record online: January 24, 2023 5213773, 2023, 10, Downloaded from https://onlinelibrary.wiley.com/doi/10.1002/anie.202218595 by University Town Of Shenzhen, Wiley Online Library on [23/11/2025]. See the Terms and Conditions (https://onlinelibrary.wiley.com/terms-and-conditions) on Wiley Online Library for rules of use; OA articles are governed by the applicable Creative Commons License